How Dysregulated Colonic Crypt Dynamics Cause Stem Cell Overpopulation and Initiate Colon Cancer

Bruce M. Boman,[1] Jeremy Z. Fields,[2] Kenneth L. Cavanaugh,[2] Arthur Guetter,[3] and Olaf A. Runquist[4]

[1]Thomas Jefferson University, Philadelphia, Pennsylvania; [2]CA*TX, Inc., Gladwyne, Pennsylvania; and Departments of [3]Mathematics and [4]Chemistry, Hamline University, St. Paul, Minnesota

Abstract

Based on investigation of the earliest colonic tissue alteration in familial adenomatous polyposis (FAP) patients, we present the hypothesis that initiation of colorectal cancer by adenomatous polyposis coli (*APC*) mutation is mediated by dysregulation of two cellular mechanisms. One involves differentiation, which normally decreases the proportion (proliferative fraction) of colonic crypt cells that can proliferate; the other is a cell cycle mechanism that simultaneously increases the probability that proliferative cells are in S phase. In normal crypts, stem cells (SC) at the crypt bottom generate rapidly proliferating cells, which undergo differentiation while migrating up the crypt. Our modeling of normal crypts suggests that these transitions are mediated by mechanisms that regulate proliferative fraction and S-phase probability. In *FAP* crypts, the population of rapidly proliferating cells is shifted upwards, as indicated by the labeling index (LI; i.e., crypt distribution of cells in S phase). Our analysis of FAP indicates that these transitions are delayed because the proliferative fraction and S-phase probability change more slowly as a function of crypt level. This leads to expansion of the proliferative cell population, including a subpopulation that has a low frequency of S-phase cells. We previously reported that crypt SC overpopulation explains the LI shift. Here, we determine that SCs (or cells having high stemness) are proliferative cells with a low probability of being in S phase. Thus, dysregulation of mechanisms that control proliferative fraction and S-phase probability explains how *APC* mutations induce SC overpopulation at the crypt bottom, shift the rapidly proliferating cell population upwards, and initiate colon tumorigenesis. [Cancer Res 2008;68(9):3304–13]

Introduction

Our long-term goal is to elucidate cellular mechanisms that link genetic changes with tissue changes during the development of colorectal cancer (CRC). This is a formidable task because colon carcinogenesis is a complex process: (*a*) it occurs in tissues (crypts) which themselves are complex; (*b*) it typically develops over a long period of time (decades), with sequential changes at many biological levels, from genes to organ systems; and (*c*) it involves a multitude of causes, contributory factors, and risk factors. To investigate these complex processes, we turned to mathematical modeling because it is a scientific method that allows one to (*a*) investigate possible kinetic mechanisms in complex chemical and biological systems (1, 2), (*b*) validate any particular mechanism or model against available biological data, and (*c*) generate plausible research questions and hypotheses for further study. In our modeling experiments, we create kinetic models that simulate the dynamics of the human colonic crypt, and we use them to study mechanisms that might be responsible for the initiation and development of CRC.

In our previous study (3), we used mathematical modeling to address a question in cancer initiation: what, in familial adenomatous polyposis (FAP), links the germline adenomatous polyposis coli (*APC*) mutation to the tissue abnormality [shift of the labeling index (LI)] in normal-appearing FAP crypts? FAP is also a good biological model for sporadic CRC because the genetic, cellular, and tissue events are similar. Results from this first generation model (3) showed that only an increase in crypt stem cell (SC) number, not changes in rates of cell cycle proliferation, differentiation, or apoptosis of non-SC populations, simulated the LI shift in FAP crypts. This led us to hypothesize that the link between APC mutation and LI shift in CRC initiation in FAP is crypt SC overpopulation. This hypothesis is plausible because mounting evidence suggests that SC are the cells of origin of colon and other cancers and because we showed (4) that increased symmetrical division of cancer SC can uniquely account for the exponential increase in SC, intermediate cell, and nonproliferative cell populations in development of CRC. We built the second generation model reported herein to investigate the next logical question: what kinetic mechanisms in FAP crypts underlie the SC overpopulation in CRC initiation?

Materials and Methods

Modeling strategy. First, we built a model (Fig. 1) that was consistent with biological data, including the LI for normal human colonic crypts. We then tested the model for its ability to predict four independent data sets (Table 1). Our approach was to show that the model accurately predicts these independent biological data sets, corroborates our SC overpopulation hypothesis, and is generally consistent with normal crypt biology. Showing this, we could then argue that the model has validity and utility for suggesting plausible kinetic mechanisms that underlie colon tumorigenesis, hypotheses to test those mechanisms, and biological experiments to validate them. Our minimal criteria for acceptability of models is provided in Supplementary Data.

Relevant biological characteristics of the human colonic crypt. The intestinal epithelium is a highly dynamic tissue that constitutes one of the largest human epithelial barriers (5–7). Histologically, the single cell-layered colonic epithelium consists of a multiplicity of crypts of Lieberkuhn (~14,000 crypts/cm^2), and the colonic epithelium is replaced every 5 d (120 h; refs. 6, 7). SCs are located at the crypt bottom and undergo self-renewal and simultaneously generate a population of transit cells that migrate upwards, proliferate, and begin differentiating to form goblet,

Note: Supplementary data for this article are available at Cancer Research Online (http://cancerres.aacrjournals.org/).

Requests for reprints: Bruce M. Boman, Helen F. Graham Cancer Center, 4701 Ogletown-Stanton Rd, Suite 1205B, Newark, DE 19713. Phone: 302-623-4540; E-mail: BrBoman@ChristianaCare.org.

doi:10.1158/0008-5472.CAN-07-2061

columnar, and other cells (8–12). Fully differentiated cells are first noted among cells near the junction of the hemispherical base of the crypt and straight wall side (13). In contrast, the majority of cells in the upper third of the crypt are terminally differentiated (TD) and are nonproliferative. It is estimated that SC in the human colonic crypt represent only a small proportion (<20 cells per crypt or <1%) of crypt cells and that these few SCs are responsible for driving crypt renewal (8–12). This is consistent with recent immunostaining studies in human colonic crypts for Musashi-1 protein, a putative SC marker, indicating that there are, on average, 19 SCs per crypt (14).

Uptake of [^{3}H]thymidine or BrdUrd by cells in human colonic crypts enables *in vivo* pulse-labeling of DNA-synthesizing S-phase cells (15–18); when plotted, this yields the LI^{Normal} (Fig. 2*A*). FAP crypts do not show any histologic changes, but their LI profile (LI^{FAP}) is shifted (peak shift from level 15 to 20) toward the crypt top (Fig. 2*C*; ref. 19). Crypts begin to show structural abnormalities (i.e., dysplasia) after a second hit at the *APC* locus during adenoma formation. Thus, the proliferative shift in FAP crypts represents the earliest known tissue change resulting from a germline *APC* mutation.

The LI profiles also indicate that there is a low fraction of cells in S phase at the bottommost levels of the crypt (6, 19). This is consistent with the fact that other (hematopoietic) SC populations have a low frequency of being in S phase (20, 21) and that, in the colon, SC reside at the crypt bottom.

Model design, equations, and computations. Our colonic crypt model design and dynamics and our modeling approach are shown in Fig. 1. Model equations are provided in Appendix A. Design of the model was based on our hypothesis that the biological LI (fraction of crypt S-phase cells or F_S) can be described by the product (Eq. 3) of two expressions—the fraction of proliferative cells (F_{PR}) times the probability that a proliferative cell is in S-phase (P_S). Because our model was designed to investigate mechanisms underlying SC overpopulation in FAP crypts, we derived a measure of cell stemness (ξ); it is described by the ratio F_{PR}/P_S (Eq. 4). This expression, where stemness is directly proportional to the proliferative fraction and inversely proportional to the probability of a proliferative cell being in S phase, is consistent with biological characteristics of SCs, which have an extended lifetime and a low frequency of being in S phase. Model assumptions and derivations of the equations can be found in Supplementary Data.

Calculation of values for equation parameters (m, n, P_S^{max}, and β) in model model F_S computations was determined empirically by convergence-fitting of Eq. 3 to the biological LI^{Normal} data of Potten et al. (6) using a nonlinear least-squares regression procedure (Mathematica software version 5.0). After the model was established using data for LI^{Normal}, it was used to fit LI^{FAP}. Statistical methods are described in Supplementary Data. We analyzed four data sets (Table 1). Whereas LI data sets from different laboratories show some heterogeneity (6, 15–19), they all show the same general pattern in normal crypts and a shift upwards in FAP crypts. The results of Potten and colleagues for LI^{Normal} (6) and LI^{FAP} (19) were used in our analysis because they are, to our knowledge, the largest series of cases analyzed, giving not only LIs but also crypt dimensions and cell proliferation data from flow cytometry.

Results

Modeling biological data for normal colonic crypts. Iteratively fitting model output (Eq. 3) to biological data for normal colonic crypts (data set 1) yielded a best-fit curve from which we obtained values for the four model parameters (see Fig. 2

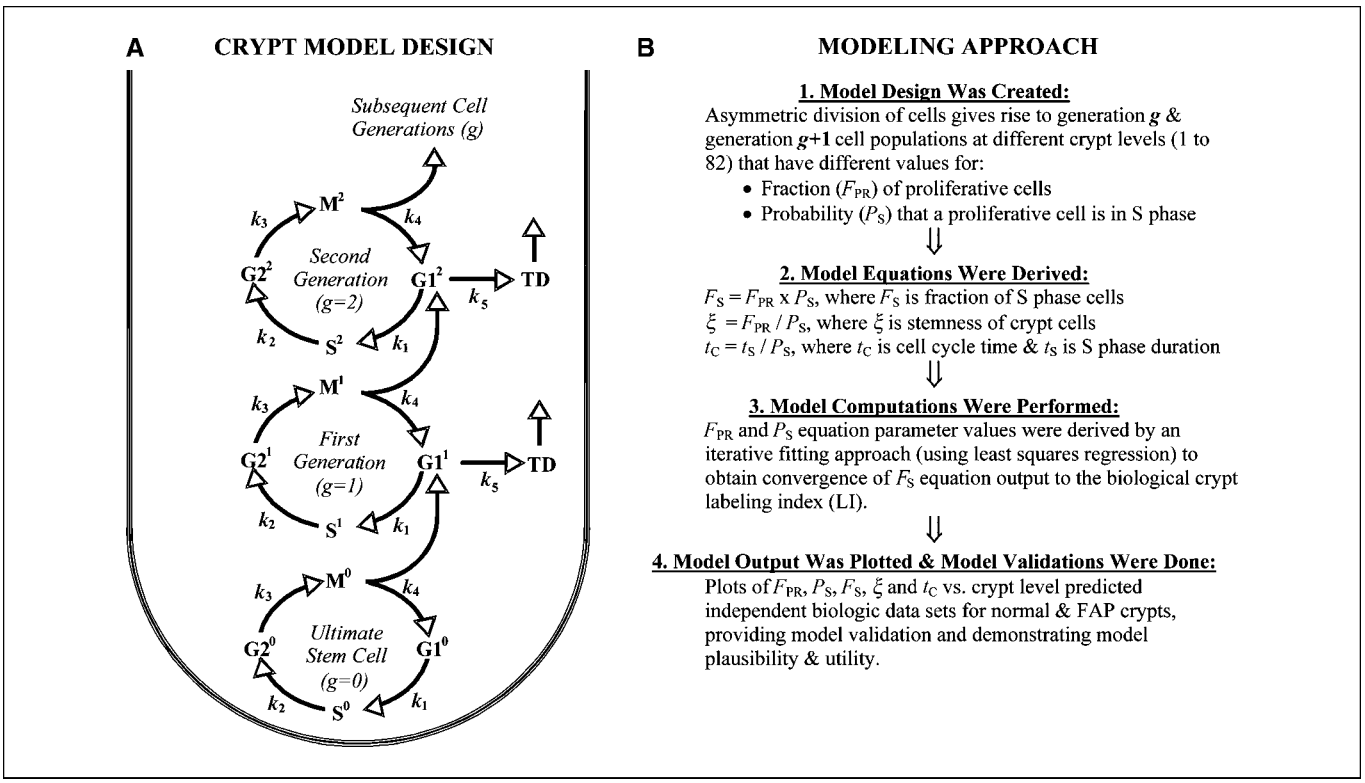

Figure 1. Colonic crypt model design and dynamics and our modeling approach. The model equations are provided in Appendix A. *A,* the model design for the dynamics of cell populations in colonic crypts. In this figure, cell cycle phases are labeled G_1^g, S^g, G_2^g, and M^g, where superscripts indicate cell generation number (g) from 0 to 81. It also depicts a pathway for G_1 cells to become TD cells. Each step in the model cell cycle is regulated by a rate constant (k_1–k_4), whereas k_5 regulates terminal differentiation. Model cell divisions are asymmetric. Each generation (g) of mitotic (M^g) cells divides to produce a new G_1^g cell identical to the original parent and a nonidentical daughter cell of the next generation (G_1^{g+1}). Each generation of cells has different properties: (*a*) different F_{PR} values due to an unequal proportion of nonproliferative cells (i.e., TD cells) and (*b*) different probabilities (P_S) of being in S phase. Thus, in each crypt cell generation at any given crypt level, P_S^g, F_{PR}^g, and the fraction of each cell type (G_1, S, G_2, M, and TD) reflect the kinetic characteristics of the subpopulation of cells at that level. *B* summarizes our modeling approach.

legend). Figure 2*A* shows a comparison of model output for S-phase fraction (F_S) with LI^{Normal} biological data. The fit was outstanding ($r^2 = 0.99$).

The parameter values were then used to plot F_{PR} and P_S versus crypt level (dashed lines of Fig. 2*B*). The product of the F_{PR} and P_S curves yields the skewed bell-shaped curve (solid line), which is identical to the F_S plot in Fig. 2*A* (note the difference in range of the *Y*-axis scale). Having successfully fitted the F_S plot to the biological LI^{Normal} data, we then tested the ability of the model to predict other independent sets of data, including SC (Fig. 3), FAP crypts (Figs. 2*C* and *D* and 4) and cell cycle times (Table 2).

The first independent data set (data set 2) we tested for goodness-of-fit using our model was biological data on immunostaining of normal colonic crypts for SC (14) using the SC marker Musashi-1 protein (22). Comparison of stemness (ξ) with the number of cells staining positive for Musashi-1 in the crypt bottom (Fig. 3*A*) shows that the modeling data (solid line) and biological data (dashed line) yield similar percentages across crypt levels 1 to 20. To make a direct and meaningful comparison of modeling data with biological data, stemness was computed as a percentage by a method analogous to the one used in the Musashi study (14). Plotting ξ versus crypt level, either as a percentage (Fig. 3*A*) or as the ratio F_{PR}/P_S (Fig. 5*A*), shows that cells at crypt levels 1 to 2 have the largest ξ value (ξ^{max}) compared with cells at all other crypt levels. Figure 5*A* shows that, at higher crypt levels, ξ exponentially decreases and approaches 0 by crypt level 40 (generation 39). Comparison of stemness (ξ) in the whole crypt with the Musashi-1 immunostaining pattern for whole colonic crypts (Fig. 3*B*) shows that the modeling and biological data sets yield similar proportions across all crypt regions: lower, middle, and upper. The Pearson product-moment correlation between (ξ) and the Musashi-1 data was strong ($r = 0.876$; $P < 0.001$). The squared correlation was 0.768, indicating that stemness explains ~75% of the variance of the Musashi-1 data. Yet, another test showed the ability of our model to predict the Musashi-1 staining data. The Kolmogorov-Smirnov test (a nonparametric test) was used to compare the two distributions. The null hypothesis that both stemness and the Musashi-1 data have the same distribution could not be rejected (exact *P* level, $P = 0.605$).

Modeling biological data for FAP colonic crypts. We then tested the model for its ability to predict a second independent data set (data set 3)—the proliferative abnormality (LI shift) in FAP. For modeling FAP crypts, Eq. 3 was again used to obtain variable values (see Fig. 2 legend) by iterative fitting to the biological data. Comparison of the model's F_S profile with the biological LI^{FAP} data is shown in Fig. 2*C*. Again, the fit was outstanding ($r^2 = 0.98$). Moreover, model output for the F_S equations for normal crypts and FAP crypts were significantly different ($P < 0.001$ by *F* test), paralleling the biological difference between normal and FAP crypts.

Plots of F_{PR} and P_S for FAP crypts are shown in Fig. 2*D*. The F_{PR} curve for FAP crypts was shifted to the right (toward the crypt top) compared with that for the normal crypt (Fig. 4*A*; $P < 0.001$), indicating that the population of proliferative cells has expanded and shifted upwards toward the crypt top. A similar right-shift was seen for the P_S curves in FAP (Fig. 4*B*; $P < 0.001$). Both of these right-shifts suggest a mechanism for the right-shift of the LI curve in FAP, namely, that in the FAP model crypt F_{PR} and P_S (and presumably their biological counterparts) change more slowly along the crypt axis.

The ability of our model to quantitatively predict these two independent data sets (Musashi-1 immunostaining in normal crypts; FAP LI) indicates to us that our model is valid. Given that stemness and the number of cells staining positive for the Musashi-1 protein were correlated, we assumed that the ξ value gives a measure, at each level, of the SC population size (technically, the size of populations of cells that have SC-like properties). Given this validity and using the model output for FAP crypts, we then used the model to predict SC-related variables in FAP crypts (for which biological data is not yet available), including stemness (ξ) and SC population size.

The plot of ξ versus crypt level for FAP crypts (Fig. 5*A*) was similar to normal crypts, with ξ being highest at the crypt bottom and an exponential-like decrease in ξ over the entire crypt length. However, comparison of the FAP and normal curves indicates that, at each crypt level, the ξ^{FAP} value is larger than the ξ^{Normal} value.

Because curves shown in Fig. 5*A* exhibit no obvious indication (e.g., a point of discontinuity or inflection point) of an SC niche, we used two other approaches to quantitatively estimate the SC population size from the two ξ curves in Fig. 5*A*. First, we determined the crypt level that corresponds to $^1/_2\xi^{max}$ using the normal curve. In the normal crypt, cells in level 1 up to and including level 6 have ξ values equal to or greater than $^1/_2\xi^{max}$ ($^1/_2\xi^{max} = 5.1$). In the FAP crypt, cells up to and including level 11 have ξ values of ≥ 5.1. Using estimates of the number of cells at each level (see Assumption 1), we calculated that FAP model crypts have 2.3 times more cells with ξ values of 5.1 or greater than do normal model crypts. Second, we determined area under the curve (AUC) for the ξ plots shown in Fig. 5*A*. The ratio of AUC^{FAP}/AUC^{Normal} should also give an estimate of the relative SC population sizes in FAP versus normal crypts. We calculated that the ratio of AUC^{FAP}/AUC^{Normal} equals 1.8. Thus, both approaches suggest that, in the FAP model crypt, (*a*) the SC population is expanded (~2-fold) in size and (*b*) the SC niche in FAP is extended about twice as far up the crypt.

Comparison of the plots of stemness (ξ in Fig. 5*A*) and S-phase cell distribution (F_S in Fig. 5*B*) for normal crypts and for FAP crypts shows that, in model FAP crypts, the extension of the ξ curve, which is both higher and right-shifted (away from the crypt bottom), is associated with a shift in the F_S curve upwards toward the crypt top.

Number of proliferative cells per crypt. In the model (Eq. 5), the total number of normal crypt proliferative cells was 1,006, whereas the total number of FAP crypt proliferative cells was found to be 1,155. Modeling data thus suggest that the proliferative cell population size has expanded by 15% in FAP crypts compared with normal crypts ($P < 0.0001$, Fisher's exact probability test).

Cell cycle rate constant values and half-life values for G_1, S, G_2, and M phase cells in the normal colonic crypt. The cell cycle rate constant values and half-life values for G_1, S, G_2, and M phase cells were estimated for the normal colonic crypt. Details on the assumptions, equations, and calculations pertaining to this analysis can be found in Supplementary Data. A summary of the results is given in Table 2. The average rate constant values for cell cycle steps and generated cell cycle phase half-life times were consistent with biological data for crypt cell cycle durations (data set 4) reported by Potten and colleagues (6), which are also listed in Table 2 for comparison.

Cell cycle time for normal and FAP crypts. The cell cycle time (t_C) as a function of crypt level for normal and FAP crypts were calculated using Eq. 6. A plot of cell cycle time for normal crypts

Table 1. Biological data sets used in our computational analysis

Data set	Data	Computational analysis	Reference
1	LI of normal colonic crypts	F_{PR}, P_S, ξ for normal crypts	(6)
2	Distribution of Musashi staining for normal colonic crypts	ξ for normal crypts	(14)
3	LI of FAP colonic crypts	F_{PR}, P_S, ξ for FAP crypts	(19)
4	Total cell cycle phase durations for normal colonic crypts	Rate constant values and $t_{1/2}$ for normal crypts	(6)

(solid line, Fig. 5*C*) shows that cells at the lowest crypt levels have the longest cell cycle times. At higher crypt levels, t_C values decreased exponentially, approaching a minimum by crypt level 40. A plot of t_C versus crypt level for FAP crypts (dashed line, Fig. 5*C*) showed a similar pattern, although, from crypt levels 1 to 30, the t_C^{FAP} values were considerably larger than the t_C^{Normal} values.

Discussion

Our previous modeling of the abnormal LI in FAP crypts implicated SC overpopulation in CRC initiation (3). In the present study, we created a second generation model to investigate what biological mechanisms in FAP crypts underlie the SC overpopulation in CRC initiation. This new model provides a description of the dynamic steady-state in normal and FAP crypts, as well as quantitative details about SC, proliferating cell, and TD cell populations. Because the product ($P_S \times F_{PR}$) computes the distribution of S-phase cells (corresponding to the biological LI) and the ratio F_{PR}/P_S computes stemness (corresponding to the distribution of Musashi-1–positive cells), we can study the dynamic relationship between crypt SC and S-phase cell populations. Thus, the new model provides a tool for examining kinetic and cellular mechanisms related to CRC development. This is important because of mounting evidence that SC are the cells of origin of CRC and other cancers.

Below, we discuss (*a*) why our model can be used with confidence as a tool to investigate changes in steady-state crypt dynamics that occur in tumor initiation, (*b*) what is the biological relevance of the mechanisms described by our model, (*c*) a corollary hypothesis on mechanisms involved in adenoma development, and (*d*) how our findings stimulate new questions about biological mechanisms involved in the non–steady-state dynamics that lead to tumor growth and development of CRC.

When using any model, it is important to show that the model is biologically reasonable (is plausible), that it accurately simulates the available biological data (is valid), and that it suggests new mechanisms and important hypotheses (is useful) that can be studied experimentally. Our model is plausible because it satisfies all criteria (see Supplementary Data) we established for a useful model of colonic crypt dynamics. For example, it computed the normal human colonic crypt S-phase profiles (data set 1) with an outstanding goodness of fit ($r^2 = 0.99$; Fig. 2*A*). Also, the proposed mechanisms involve gradients of F_{PR} and P_S, and we (23) and others (24, 25) found that APC and other factors critical to colon tumorigenesis are distributed as gradients along the crypt axis.

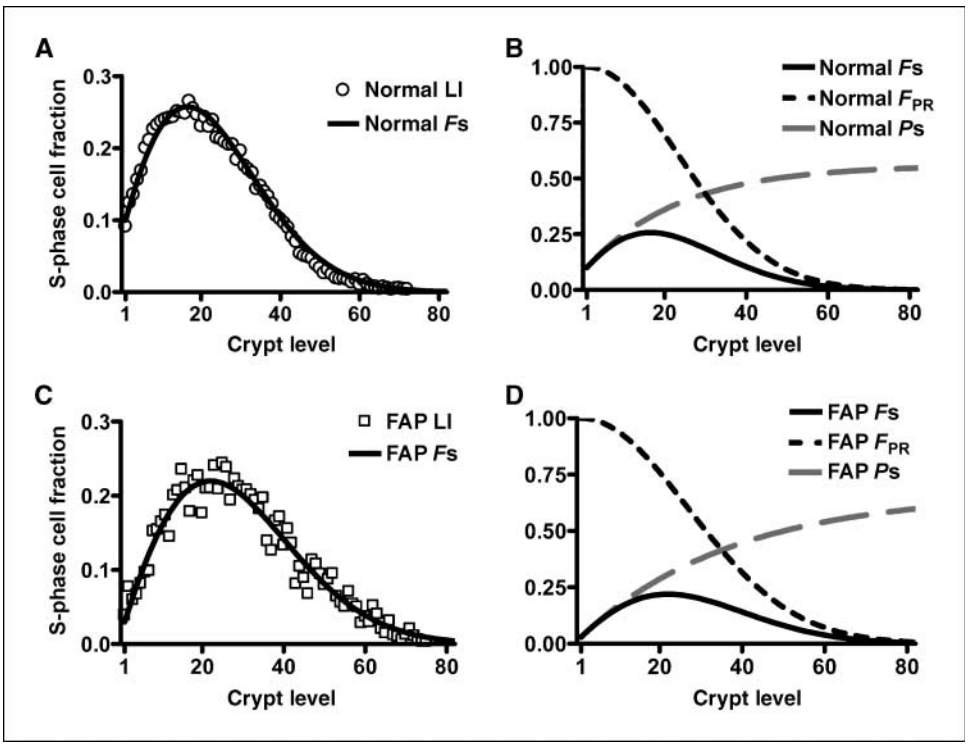

Figure 2. *A* shows a plot of the of S-phase cell distribution (F_S) computed from the model for the normal crypt (*solid line*) and the biological LI data for normal colonic crypts [*open circles*; data from Potten and colleagues (6)], both as a function of crypt level. Crypt level 1 corresponds to the crypt bottom; level 82 to the crypt top. Values obtained (from standard nonlinear least squares regression analysis) for parameters in the F_S equation were $P_S^{max} = 0.56$; $\beta = 0.10$; $m = 0.044$; $n = 0.0010$ for normal crypts. The computed curve has a high goodness of fit ($r^2 = 0.99$) with the biological data. *B* shows a plot of F_{PR} (descending dashed line) and P_S (ascending dashed line); the product of the F_{PR}^g and P_S^g curves yields the skewed bell-shaped curve (*solid line*), which is the same as the F_S plot in *A* (note the difference in range of the *Y*-axis scale). *C* is similar to *A* except that the plots are the computational (*solid line*) and biological data (*open squares*; ref. 19) for FAP crypts rather than normal crypts. For FAP crypts, parameter values obtained by iterative fitting of Eq. 3 to the biological data were $m = 0.017$; $n = 0.00082$; $P_S^{max} = 0.67$; $\beta = 0.034$. In *C*, the F_S curve shows high goodness of fit with the biological data ($r^2 = 0.98$). *D* is similar to *B*, except that *D* is for FAP crypts.

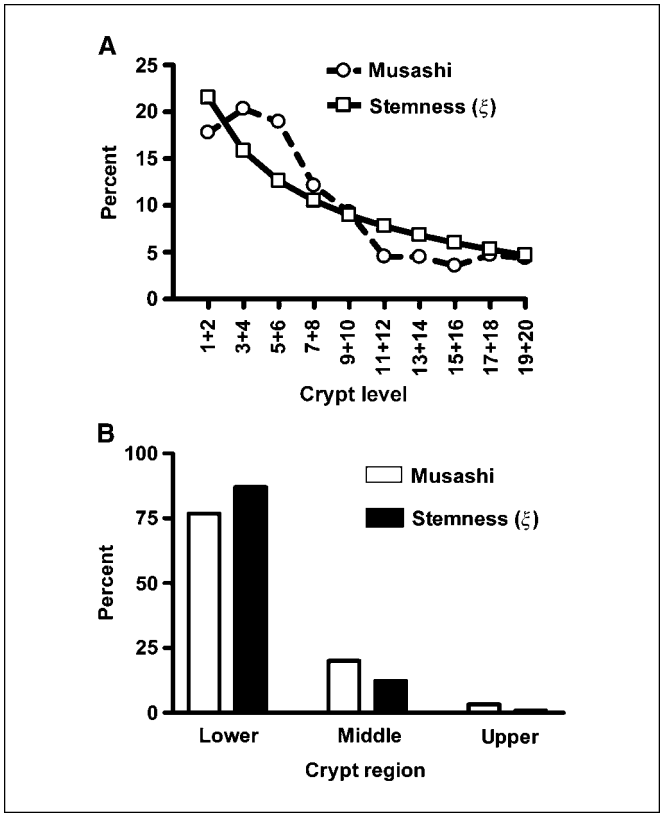

Figure 3. *A* shows the distributions for normal crypt levels 1 to 20 of stemness (*solid line*) and distribution of Musashi-1 staining (*dashed line*; from ref. 14). To compute the ξ curve here, we used an approach that was comparable with that of Nishimura (14) who plotted percentage of total number of Musashi–positive cells for pairs of crypt levels (1–2, 3–4, 5–6, etc.) ranging from levels 1 to 20. Here, we first determined the ratio F_{PR}/P_S from modeling data for normal crypts and plotted it versus individual crypt levels (shown as solid line in Fig. 5*A*) and then we calculated total crypt stemness (AUC). We then replotted the stemness curve for pairs of crypt levels as a percentage of total stemness (shown as solid line in *A*). Model stemness was highly correlated ($P < 0.05$) with Musashi-1 positivity ($r = 0.88$; $P < 0.001$). *B* shows, for the whole normal crypt, both the stemness (*filled columns*) computed from the model (area under the ξ curve) and the distribution of immunostaining positivity for the Musashi-1 protein, a putative SC marker (*unfilled columns*; from ref. 14). Both variables show similar proportions (of crypt cells) across lower, middle, and top crypt regions.

The model seems to be valid because it predicts results for four independent data sets: (*a*) the Musashi immunostaining profile for SCs (data set 2), (*b*) normal crypt cell cycle durations (data set 4), (*c*) the longer cell cycle time (t_C) at the crypt bottom (6, 26), and (*d*) the FAP crypt LI (data set 3).

The model seems to be useful because it suggested (*a*) a cellular mechanism, (*b*) an important new hypothesis regarding CRC initiation, and (*c*) a new definition for SC. The mechanism suggested by the model is that SC overpopulation (~2-fold for normal-appearing FAP crypts) links the earliest genetic change (*APC* mutation) and earliest tissue abnormality (LI shift) in CRC initiation. This was independently predicted by our first generation model (3) and is consistent with other findings: (*a*) our recent biological observations (23) that in FAP crypts the number of colonocytes that have a crypt base cell phenotype (which includes SC) is increased 1.5-fold to 2.2-fold; (*b*) the finding that there is an increase in Musashi-1 expression in intestinal tumors in Apc^{Min} mice, a mouse model of FAP (22); (*c*) findings of another modeling study on gene methylation diversity patterns in FAP crypts implicating increased SC numbers in FAP crypts (27).

In our new hypothesis, CRC initiation is caused by dysregulation of the above two kinetic mechanisms in the crypt, which become altered when *APC* is mutant—one mechanism regulates F_{PR} and the other regulates P_S. The new definition is that SC or cells with a high degree of stemness are proliferative cells with a low probability of being in S phase—a property that can be quantified and has biological relevance. Although other valuable models have been developed to study cellular dynamics in intestinal crypts (summarized in ref. 28), to our knowledge, our models (this paper and ref. 3) are the first designed to investigate the cellular etiology of the proliferative abnormality in normal-appearing FAP crypts. In comparison, the recent model by Johnston et al. (28) was designed to simulate the dynamics of a single colonic crypt using a compartmental approach. It showed that increased cell renewal, which is equivalent to reduced apoptosis or differentiation, can explain the growth of cancers. Their model, as did our recent model on fully-developed CRC (4), predicted the long lag-phase in tumor growth.

These considerations strongly suggest that our current model has plausibility, validity, and utility. It can thus be used with confidence for generating hypotheses to be tested in biological studies or to do further modeling studies aimed at explaining existing biological data. Given our modeling results, four points bear further discussion.

The biological relevance of stemness (ξ) as defined by the ratio F_{PR}/P_S. In our model, cells with high stemness have a high probability for being a proliferative cell (high F_{PR}) and a low probability for being in S phase (low P_S). This is consistent with two known properties of SC—they proliferate only slowly but can do so indefinitely (29). Consistent with SC retaining a high F_{PR} is the fact that human colonic SC divide over the entire lifetime of an individual (~5,000 times; ref. 10). Consistent with SC having a relatively slow cell cycle time is the fact that the cycle time for cells in the lower crypt (where SC reside) is significantly longer than times for proliferative cells higher up the crypt (6, 26, 30, 31). Indeed, our modeling predicted that cells at the crypt bottom have the longest cell cycle time (Fig. 5*C*). Because the cell cycle time at

Table 2. Average cell cycle rate constants and cell cycle phase half-life values for the entire cell population in normal colonic crypts

Rate constant	Average value (h^{-1})	Cell phase	Average $t_{1/2}$ (h)	Average cell cycle phase duration (h)*
k_1	0.050	G_1	14	17
k_2	0.074	S	9.4	8.8
k_3	0.17	G_2	4.1	4.0
k_4	2.0	M	0.35	0.32
k_5	0.050			
		Total time	28	30

NOTE: Details on the assumptions, equations, and calculations pertaining to this analysis can be found in Supplementary Data.
*Biologically determined (6).

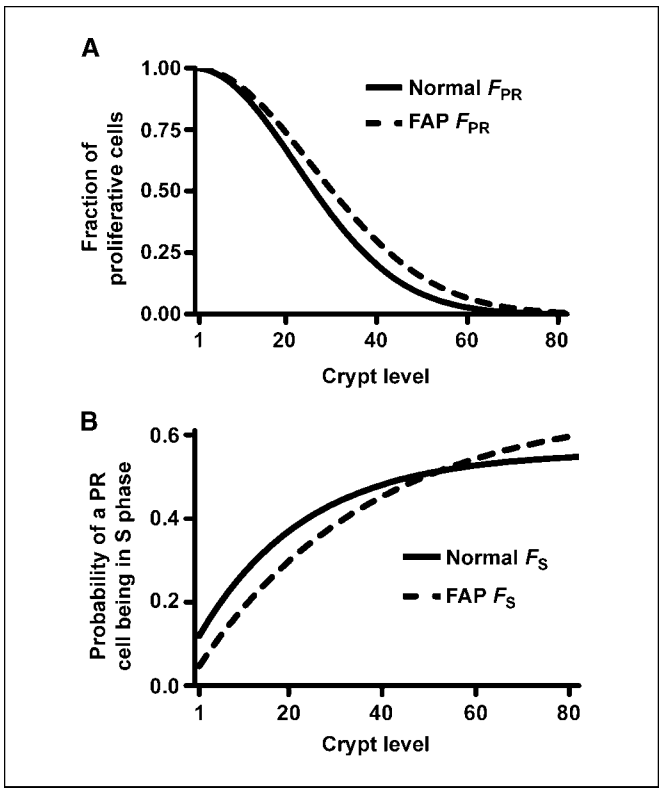

Figure 4. *A* shows the fraction (F_{PR}) of crypt cells that are proliferative cells at each crypt level for normal (*solid line*) and FAP (*dashed line*) model crypts. *B* shows for normal (*solid line*) and FAP (*dashed line*) model crypts the probability (P_S) that a proliferative cell at each crypt level is in S phase. The right-shifting of the FAP curves (both are significantly different, $P < 0.001$) indicates that in FAP, F_{PR} and P_S change more slowly with increasing cell generation number.

level 1 is ~100 hours and, in our model, level 1 corresponds to a single cell that is an SC, we predict that a normal colonic SC has a cell cycle time of ~100 hours. This cell cycle time of ~100 hours is about thrice as long as the average cell cycle time (30 hours; see Table 1) for the entire crypt. The important point from the modeling data on the FAP curve in Fig. 5*C* is that the even longer cell cycle time in FAP crypts correlates with our finding that the SC population is expanded (~2-fold) in size in the FAP crypt.

A longer cell cycle time and a low P_S for SC could both be explained if SC have a prolonged G_1 phase or arrest in G_0. A prolonged G_1 phase has also been described for hematopoietic SC (32). Identifying biochemical and cellular pathways that might maintain these two SC properties should provide clues regarding how SC retain stemness and how SC population size is maintained.

Our modeling indicates that ξ is highest at the crypt bottom and exponentially decreases along the crypt axis toward 0 at the crypt top (Fig. 5*A*). This gradient parallels the distribution of cells staining positively for the Musashi protein, a marker for individual SC (Fig. 3*A*). This gradient may be explained in two quite different ways: (*a*) decreases in the degree of stemness per individual cell and/or (*b*) decreases in the proportion of crypt cells, at any given crypt level, that are SC. The first explanation that stemness decreases incrementally is consistent with radiobiological experiments (10, 11, 26), showing that the highest degree of stemness is associated with enterocytes at the crypt bottom and that there is a gradual loss of stemness in cells at higher levels within the lower crypt. Indeed, based on these data, Potten argued that stemness decreases incrementally in the crypt. Furthermore, evidence indicating that a single SC at the crypt bottom gives rise to progenitor cells, which have SC-like properties (e.g., self renewal) and are committed to generate a particular cell lineage (7, 8), supports the notion that there are incremental decreases in the degree of stemness in cells along the crypt axis.

In the second explanation, decreases in stemness upwards along the crypt axis simply reflect a decrease in the proportion of cells at

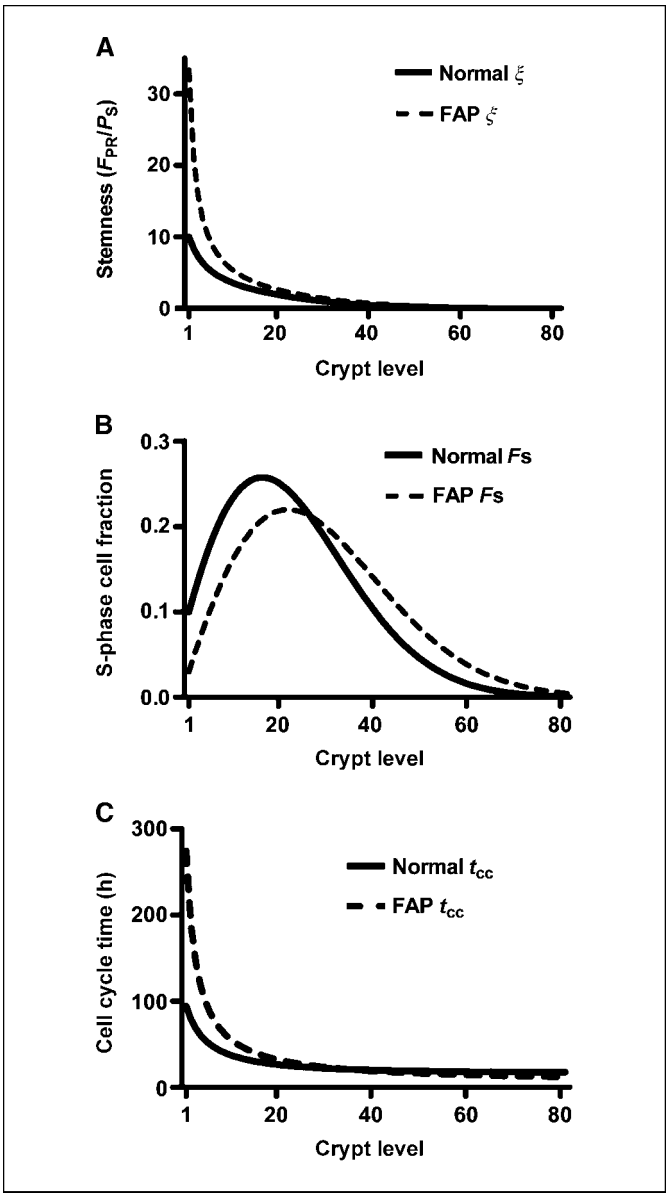

Figure 5. *A* shows the stemness value (ξ), at each crypt level, computed from the model for normal (*solid line*) and FAP crypts (*dashed line*), where $\xi = F_{PR}/P_S$. *B* shows the S-phase cell distribution (F_S) computed from the model for the normal crypt (*solid line*) and the FAP crypt (*dashed line*). Compared with normal crypts, the ξ curve is both higher and right-shifted (away from the crypt bottom) in model FAP crypts (*A*) and is associated with a parallel right-shift of the F_S curve (upwards toward the crypt top; *B*). *C* shows the cell cycle time (t_C) values for normal and FAP crypts. t_C for normal crypts (*solid line*) shows that cells at the lowest crypt levels have the longest cell cycle times. A plot of t_C versus crypt level for FAP crypts (*dashed line*) showed a similar pattern, although from crypt levels 1 to 30 the t_C^{FAP} values were larger than and right-shifted from the t_C^{Normal} values.

any given crypt level that are SC. This explanation is consonant with the idea that, as argued by others (33), being an SC is an all-or-none phenomenon. This is also consistent with the pattern of Mushashi-1 staining—there were fewer stained cells at higher crypt levels, but staining only identified isolated individual cells (presumed to be SC). If, indeed, Musashi-1 is an SC marker that identifies individual SC, then the idea that stemness incrementally decreases along the crypt axis would seem unlikely.

Because our model computes ξ per crypt level, it is compatible with either explanation for decreased stemness. The important finding here is that both the model results and the Musashi results support the notion that stemness or SC numbers decrease exponentially along the normal crypt axis. Identifying how stemness changes in quantity and/or distribution is crucial to our understanding of how, biologically, changes in SC populations might affect the dynamics of other cell populations in the colonic crypt, particularly those dynamics involved in CRC development.

Possible biochemical and cellular pathways corresponding to normal regulation of F_{PR} and P_S. Because in our modeling of FAP crypts we found that F_{PR} and P_S are altered and because FAP crypts have a cancer-initiating germline *APC* mutation, it seems likely that some aspects of APC signaling are the biological counterparts to regulation of F_{PR} and P_S in the model. Indeed, APC is a tumor and growth suppressor protein with many functional domains and associated cellular functions. Knowing how F_{PR} and P_S change along the crypt axis in the model should give us clues as to which APC pathways correlate with F_{PR} and P_S gradients and which are important in the regulation of SC population size. A prime candidate is the ability of APC to down-regulate β-catenin/TCF-4 signaling. For one thing, in Tcf-4 knockout mice, the intestinal SC population is depleted (34). For another, APC concentrations form a gradient—negligible at the normal crypt bottom and increased toward the crypt top (24, 25)—while β-catenin localization to the nucleus, which leads to TCF-4 activation, selectively occurs in cells at the bottom of normal crypts (35, 36). Thus, the decline in TCF-4 activation upward, along the crypt axis, roughly parallels the declining F_{PR} gradient in the model—both are inverse to the APC gradient.

How might the decline in TCF-4 activity lead to a decline in the proliferative capacity of colonocytes along the crypt axis? TCF-4 activity occurs through its regulation of the expression of many genes—some are up-regulated; others are down-regulated. For example, our recent studies (37, 38) and those of others (39) suggest that survivin signaling may be particularly important. Activation of TCF-4 increases survivin expression, which is consistent with our finding that its expression is also restricted to the crypt bottom (23, 37). Survivin is an antiapoptotic protein and also promotes cell proliferation by binding to and activating aurora B kinase, which is necessary for chromosome segregation and cytokinesis during mitosis. Consequently, survivin, by preventing apoptosis and catalyzing mitosis, maintains the cell at a high proliferative potential. Therefore, expression of survivin in colonocytes at the crypt bottom may be one biochemical mechanism that corresponds to high F_{PR} and high stemness (F_{PR}/P_S) at the crypt base in our model.

Mechanisms underlying SC overpopulation and the LI shift in FAP crypts. In our model, increased stemness is a result of kinetic changes involving F_{PR} and P_S. Specifically, in the lower half of model FAP crypts, F_{PR} and P_S change more slowly with increasing cell generation number. These changes cause the ξ curve (Fig. 5*A*) to be both higher and right-shifted (away from the crypt bottom). This change in the ξ curve is associated with a parallel shift of the F_S curve (corresponding to the LI shift; Fig. 5*B*). These observations suggest that dysregulation of the mechanisms that control the biological counterparts of F_{PR} and P_S cause increased stemness, which causes the right shift of the LI in FAP.

A crucial point is that although, biologically, SC must be proliferative cells (corresponding to high F_{PR}), they would not likely be labeled by the pulse-labeling (using BrdUrd or [^{3}H]thymidine) typically used to determine the LI because SC are cells that cycle only slowly (26, 29–31). In contrast, SC progeny that have lost most of their stemness will readily be labeled by pulse-labeling because they are rapidly proliferating. Therefore, an expansion of the SC population away from the crypt bottom in FAP (as predicted by our modeling) will cause the population of cells that undergo pulse-labeling to be shifted toward the crypt top.

If dysregulation of the kinetic mechanisms that regulate the biological counterparts of F_{PR} and P_S occurs in FAP, then understanding how dysregulation of APC-mediated signaling pathways (discussed above) might correspond to alterations in F_{PR} and P_S could clarify how CRC initiation might occur. For example, when *APC* is mutant, β-catenin/TCF-4 signaling would not be inhibited as much as in normal crypts. In this case, survivin expression would not be inhibited to the same extent and there would be more proliferative cells due to inhibition of apoptosis and promotion of mitosis. This could correspond to the increase ($\sim$15%) in the number of proliferative cells found for model FAP crypts. Dysregulation of the β-catenin/TCF-4/survivin pathway is consistent with the fact that normal-appearing FAP crypts have (*a*) expansion of the cell population expressing survivin from the crypt bottom into the middle region (23), (*b*) a reduced number of apoptotic cells (40), and (*c*) a greater number of mitotic figures (41). These considerations suggest that dysregulation of mechanisms in the colon corresponding to regulation of F_{PR} and P_S in our model causes expansion of the SC population at the crypt bottom, which shifts the distribution of the rapidly proliferating cell population toward the crypt top.

How our modeling enhances understanding of CRC development and colon cancer SC. Our current study is relevant to development of CRC because most cases of colonic adenomas and carcinomas have acquired mutations in the *APC* gene. It is also relevant to colon cancer SC because of recent findings on SC in CRCs. It is well known that the total number of cells is exponentially increased in CRC (from 2×10^3 cells in normal crypts to 10^8–10^{13} cells in a CRC). It was recently found that CRCs contain a small but significant proportion (0.25–2.5%) of tumor cells that are cancer SC (42, 43). Therefore, it can be deduced that the size of the SC subpopulation in those tumors has also increased exponentially (from $\sim$20 SC in a normal crypt to 10^6–10^{11} cancer SC in a CRC), and this must have occurred during the various phases of colon tumorigenesis (4). Below, we discuss these phases and some possible mechanisms.

The studies in the present paper on the earliest tissue abnormality in FAP crypts not only implicate SC overproduction ($\sim$2×) in CRC initiation, but also suggest other mechanisms underlying CRC development. For example, our modeling shows that, whereas FAP crypts have more proliferative cells than normal crypts, FAP crypt cells do not have a shorter cell cycle time than normal crypt cells, but rather a longer one (Fig. 5*B*). Extrapolation of these findings leads to the prediction that, as tumors develop,

the proportion of proliferative cells (proliferative fraction) will increase compared with normal tissues. Thus, model predictions are consistent with the idea that tumors have increased proliferation because of an increased number of proliferative cells, not because of a decreased cell cycle time (44). This has implications in cancer treatment because cytotoxic chemotherapy is often designed to kill actively cycling cells.

Biological evidence also suggests that the concepts and mechanisms of our hypothesis on SC overpopulation may apply to some aspects of adenoma development. Morphologically, adenomatous crypts are wider and longer than normal crypts (45), which indicates that the total crypt cell population has expanded. Adenomatous epithelium has a relatively immature, undifferentiated phenotype that resembles the proliferative epithelium found in the bottom one-third of normal crypts (46), suggesting that the proliferative cell population expands to replace the entire crypt population. LIs show that the distribution of S-phase cells is shifted upward to the luminal surface of adenomatous crypts (47, 48), which suggests that the rapidly proliferating cell population is displaced toward the crypt top. To explain these observations, particularly the shift of the LI to the crypt top, we present a corollary to our SC overpopulation hypothesis: as the crypt SC population continues to expand after cancer initiation, it will cause a futher displacement of the rapidly proliferating cell population and a further shift in the distribution of S-phase cells (LI) toward the crypt top. This prediction is testable by immunohistochemical staining of colon tissue sections using antibodies against available colonic and intestinal SC markers, such as CD133 (42, 43), CD44 (49), or Lgr5 (50), and against rapidly proliferating cells (e.g., Ki67).

Because CRCs do not have definable crypt structures and have mutations in many other genes in addition to *APC* mutations, it is less clear how our concepts and mechanisms apply to fully-developed colon carcinomas. Whereas recent studies describe the existence of colon cancer SC and provide data indicating that the tumor SC population has exponentially expanded, they do not provide mechanisms as to how SC numbers increase in CRC. Although the mechanisms described herein and our definition of stemness (F_{PR}/P_S) pertain to dynamics of colonic crypts, they also stimulate interesting new questions about mechanisms involved in exponential growth of SC and other cell populations in later phases of colon carcinogenesis.

To identify mechanisms that give rise to this exponential growth in CRC, we did a study using a different model (4), one which simulates the non–steady-state dynamics of tumor growth and provides numbers of colonic SC as a function of time. Our results showed that only an increase in symmetrical SC division can explain how both SC and non-SC populations grow exponentially in CRC. Whereas the mechanisms of our two models (this manuscript and ref. 4) are different, it is useful to see how they might interrelate because each provides an explanation for how the proliferative cell population expands during CRC development. For example, if it turns out that our definition of stemness (F_{PR}/P_S) is not limited to just normal and FAP colonic crypt SCs but also applies to colon cancer SCs, it would provide insight into cellular mechanisms involved in symmetrical and asymmetrical division of cancer SCs. The prediction that our definition for SC applies to colon cancer SC could be experimentally tested. One way could involve isolation of colon cancer SC using available colonic SC markers (42, 43, 49, 50) and determining if they have a low frequency of being in S-phase compared with proliferative non-SCs. This could be done in an analogous fashion to experiments where SC markers were used to isolate normal hematopoietic SCs, which were found by flow cytometry to have a low frequency of being in S phase (20, 21).

If it is biologically validated that our definition of stemness (F_{PR}/P_S) applies to colon cancer SC, it would indicate that symmetrical cancer SC division generates two identical daughter cells that are both proliferative cells with the same low probability for being in S phase as the parent SC. It would also indicate that if symmetrical cancer SC division were increased, it would lead to expansion of a subpopulation of proliferative cells in CRCs that has a low frequency of cells in S phase. And the expansion of such a subpopulation would, through asymmetrical cell division (as modeled in our current study), also lead to expansion of the rapidly proliferating cell population. Together, these expansions would lead to an expansion of the total proliferative cell population and drive tumor growth.

Appendix A. Model Equations

Given below are the equations used in our model. Derivations for these equations can be found in Supplementary Data.

Fraction of cells being a proliferative cell (F_{PR}). The following expression describes F_{PR}:

$$F_{PR} = \frac{\#\ \text{Proliferative cells}}{\text{Total}\ \#\ \text{cells}}.$$

The following equation describes F_{PR} at each crypt level (L):

$$F_{PR}^{L} = e^{-n(g^2)}, \qquad \text{[Eq. 3]}$$

wherein g is cell generation and n is a constant. As stated in assumption A5 (see Supplementary Data), cell generation 0 corresponds to crypt level 1 and $g = L - 1$.

Probability that a proliferative cell is in S phase (P_S). The following expression describes P_S:

$$P_S = \frac{\#\ \text{S phase cells}}{\#\ \text{Proliferative cells}}.$$

The following equation describes P_S at each crypt level (L):

$$P_S^{L} = P_S^{\max} - (P_S^{\max} - \beta)e^{-mg}, \qquad \text{[Eq. 5]}$$

wherein m is a constant, $P_S^{\max}$ is the maximum value of P_S, and $\beta = P_S^{g}$ when $g = 0$.

Note that this equation is not an expression of the probability that a cell in G_1 phase will enter S phase.

Fraction of crypt cells in S phase (F_S). The following deduction shows that the fraction (F_S) of all cells (including TD cells) that are in S phase equals the product of F_{PR} and P_S. From the above expressions for F_{PR} and P_S,

$$F_{PR} \times P_S = \frac{\#\ \text{Proliferative cells}}{\text{Total}\ \#\ \text{cells}} \times \frac{\#\ \text{S phase cells}}{\#\ \text{Proliferative cells}} = \frac{\#\ \text{S phase cells}}{\text{Total}\ \#\ \text{cells}}.$$

Thus,

$$F_{PR} \times P_S = \frac{\#\text{ S phase cells}}{\text{Total }\#\text{ cells}} = F_S.$$

The following equation describes F_S at each crypt level (L) based on the product of Eqs. 3 and 5:

$$F_S^L = (e^{-n(g^2)})(P_S^{max} - (P_S^{max} - \beta)e^{-mg}), \quad \text{[Eq. 7]}$$

Stemness (ξ). The following expression defines a measure of stemness (ξ) as the ratio F_{PR}/P_S.

$$\xi = (F_{PR})/(P_S).$$

The following equation describes ξ at each crypt level (L) based on the ratio of Eqs. 3 and 5:

$$\xi^L = (e^{-n(g^2)})/(P_S^{max} - (P_S^{max} - \beta)e^{-mg}), \quad \text{[Eq. 8]}$$

Note that the SC niche is defined as the crypt region in which cells have a ξ value equal to or greater than 1/2 ξ^{max} for normal crypts.

Total number of proliferative cells (#PR).

$$\#PR/\text{crypt} = \Sigma_0^{81}[(F_{PR}^g)(\#\text{ cells/g})] \quad \text{[Eq. 10]}$$

This equation describes the total number of proliferative (#PR) cells per crypt, where Σ_0^{81} is the sum of all F_{PR} values from generations 0 to 81.

Cell cycle time (t_C).

$$t_C = t_S/P_S \quad \text{[Eq. 11]}$$

This equation describes the cell cycle time, t_C, for the subpopulation of cells at each crypt level, where t_S is the S phase time (8.8 hours).

Acknowledgments

Received 6/3/2007; revised 2/22/2008; accepted 3/14/2008.

The costs of publication of this article were defrayed in part by the payment of page charges. This article must therefore be hereby marked *advertisement* in accordance with 18 U.S.C. Section 1734 solely to indicate this fact.

References

1. Moore JW, Pearson RG. Kinetics and Mechanism. New York: Wiley & Sons; 1981. p. 284–327.
2. Wastney ME, Patterson BH, Linares OA, Greif PC, Boston RC. The Steps in Building a Model. In: Investigating biological systems using modeling. San Diego: Academic Press; 1999. p. 11–8.
3. Boman BM, Fields JZ, Bonham-Carter O, Runquist O. Computer modeling implicates stem cell overproduction in colon cancer initiation. Cancer Res 2001;61:8408–11.
4. Boman BM, Wicha M, Fields JZ, Runquist O. Symmetric division of cancer stem cells-a key mechanism in tumor growth that should be targeted in future therapeutic approaches. Clin Pharmacol Ther 2007;81:893–8.
5. Leeson TS, Leeson CR. In: Histology. Philadelphia: WB Saunders Co; 1970. p. 309–10.
6. Potten CS, Kellett M, Roberts SA, Rew DA, Wilson GD. Measurement of *in vivo* proliferation in human colorectal mucosa using bromodeoxyuridine. Gut 1992;33:71–8.
7. Cheng H, Bjerknes M, Amar J. Methods for the determination of epithelial cell kinetic parameters of human colonic epithelium isolated from surgical and biopsy specimens. Gastroenterology 1984;86:78–85.
8. Cheng H, Leblond CP. Origin, differentiation and renewal of the four main epithelial cell types in the mouse small intestine: III. Entero-endocrine cells. Am J Anat 1974;141:503–19.
9. Winton DJ, Ponder BA. Stem-cell organization in mouse small intestine. Proc R Soc Lond B Biol Sci 1990;241:13–8.
10. Booth C, Potten CS. Gut instincts: thoughts on intestinal epithelial stem cells. J Clin Invest 2000;105:1493–9.
11. Roberts SA, Hendry JH, Potten CS. Deduction of the clonogen content of intestinal crypts: a direct comparison of two-dose and multiple-dose methodologies. Radiat Res 1995;141:303–8.
12. Brittan M, Wright NA. Stem cell in gastrointestinal structure and neoplastic development. Gut 2004;53:899–910.
13. Lorenzsonn V, Trier JS. The fine structure of human rectal mucosa. Gastroenterology 1968;55:88–101.
14. Nishimura S, Wakabayashi N, Toyoda K, Kashima K, Mitsufuji S. Expression of Musashi-1 in human normal colon crypt cells. Dig Dis Sci 2003;48:1523–9.
15. Deschner EE, Lewis CM, Lipkin M. *In vitro* study of human epithelial cells: I. Atypical zone of H3-thymidine incorporation in mucosa of multiple polyposis. J Clin Invest 1963;42:1922–8.
16. Bleiberg H, Mainguet P, Galand P. Cell renewal in familial polyposis. Comparison between polyps and adjacent healthy mucosa. Gastroenterology 1972;63:240–5.
17. Iwana T, Utsunomiya J, Sasaki J. Epithelial cell kinetics in the crypts of familial polyposis of the colon. Jpn J Surg 1977;7:230–4.
18. Lipkin M, Blattner WE, Fraumeni JF, Lynch HT, Deschner E, Winawer S. Tritiated thymidine labeling distribution as a marker for hereditary predisposition to colon cancer. Cancer Res 1983;43:1899–904.
19. Potten CS, Kellett M, Rew DA, Roberts SA. Proliferation in human gastrointestinal epithelium using bromodeoxyuridine *in vivo*: data for different sites, proximity to a tumor, and polyposis coli. Gut 1992;33:524–9.
20. Cheshier SH, Morrison SJ, Liao X, Weissman IL. *In vivo* proliferation and cell cycle kinetics of long-term self-renewing hematopoietic stem cells. Proc Natl Acad Sci U S A 1999;96:3120–5.
21. Randall TD, Weissman IL. Characterization of a population of cells in the bone marrow that phenotypically mimic hematopoietic stem cells: resting stem cells or mystery population? Stem Cells 1998;16:38–48.
22. Potten CS, Booth C, Tudor GL, et al. Identification of a putative intestinal stem cell and early lineage marker; musashi-1. Differentiation 2003;71:28–41.
23. Boman BM, Walters R, Fields JZ, et al. Colonic crypt changes during adenoma development in FAP: immunohistochemical evidence for expansion of the crypt base cell population. Am J Pathol 2004;165:1489–98.
24. Miyashiro I, Senda T, Matsumine A, et al. Subcellular localization of the APC protein: immunoelectron microscopic study of the association of the APC protein with catenin. Oncogene 1995;11:89–96.
25. Smith KJ, Johnson KA, Bryan TM, et al. The APC gene product in normal and tumor cells. Proc Natl Acad Sci U S A 1993;90:2846–50.
26. Bach SP, Renehan AG, Potten CS. Stem cells: the intestinal stem cell as a paradigm. Carcinogenesis 2000;21:469–76.
27. Kim KM, Calabrese P, Tavare S, Shibata D. Enhanced stem cell survival in familial adenomatous polyposis. Am J Pathol 2004;164:1369–77.
28. Johnston MD, Edwards CM, Bodmer WF, Maini PK, Chapman SJ. Mathematical modeling of cell population dynamics in the colonic crypt and in colorectal cancer. Proc Natl Acad Sci U S A 2007;104:4008–13.
29. Reya T, Morrison SJ, Clarke MF, Weissman IL. Stem cells, cancer, and cancer stem cells. Nature 2001;414:105–11.
30. Potten CS, Owen G, Booth D. Intestinal stem cells protect their genome by selective segregation of template DNA strands. J Cell Sci 2002;115:2381–8.
31. Kim SJ, Cheung S, Hellerstein MK. Isolation of nuclei from label-retaining cells and measurement of their turnover rates in rat colon. Am J Physiol Cell Physiol 2004;286:C1464–73.
32. D'Urso G, Datta S. Cell cycle control, checkpoints, and stem cell biology. In: Marshak DR, Gardner RL, Gottlieb D, editors. Stem cell biology. New York: Cold Spring Harbor Laboratory Press; 2001. p. 61–95.
33. Ro S, Rannala B. Methylation patterns and mathematical models reveal dynamics of stem cell turnover in the human colon. Proc Natl Acad Sci U S A 2001;98:10519–21.
34. Korinek V, Barker N, Moerer P, van Donselaar E, Huls G, Peters PJ. Depletion of epithelial stem cell compartments in the small intestine of mice lacking Tcf4. Nat Genet 1998;19:379–83.
35. Fodde R, Smits R, Clevers H. APC, signal transduction and genetic instability in colorectal cancer. Nat Rev Cancer 2001;1:55–67.
36. van de Wetering M, Sancho E, Verweij C, et al. The β-catenin/TCF-4 complex imposes a crypt progenitor phenotype on colorectal cancer cells. Cell 2002;111:241–50.
37. Zhang T, Otevrel T, Gao ZQ, et al. Evidence that APC regulates survivin expression: a possible mechanism contributing to the stem cell origin of colon cancer. Cancer Res 2001;62:8664–7.
38. Boman BM, Zhang T, Fields JZ. Correspondence: evidence that APC regulates survivin expression: a possible mechanism contributing to the stem cell origin of colon cancer. Cancer Res 2004;64:776–9.

39. Kim PJ, Plescia J, Clevers H, Fearon ER, Altieri DC. Survivin and molecular pathogenesis of colorectal cancer. Lancet 2003;362:205–9.

40. Bedi A, Pasricha PJ, Akhtar AJ, et al. Inhibition of apoptosis during development of colorectal cancer. Cancer Res 1995;55:1811–6.

41. Mills SJ, Mathers JC, Chapman PD, Burn J, Gunn A. Colonic crypt cell proliferation state assessed by whole crypt microdissection in sporadic neoplasia and familial adenomatous polyposis. Gut 2001;48:41–6.

42. Ricci-Vitiani L, Lombardi DG, Pilozzi E, et al. Identification and expansion of human colon-cancer-initiating cells. Nature 2007;445:111–5.

43. O'Brien CA, Pollett A, Gallinger S, Dick JE. A human colon cancer cell capable of initiating tumour growth in immunodeficient mice. Nature 2007;445:106–10.

44. Pierce GB. The pathology of cancer. In: McKinnel RG, Parchment RE, Perantoni AO, Pierce GB, editors. The biological basis of cancer. New York: Cambridge Univ Press; 1998. p. 14–48.

45. Wiebecke B, Brandts A, Eder M. Epithelial proliferation and morphogenesis of hyperplastic adenomatous and villous polyps of the human colon. Virchows Arch A Path Anat Histol 1974;364:35–49.

46. Lane N, Lev R. Observations on the origin of adenomatous epithelium of the colon. Cancer 1963;16:751–64.

47. Lightdale C, Lipkin M, Deschner E. *In vivo* measurements in familial polyposis: kinetics and location of proliferating cells in colonic adenomas. Cancer Res 1982;42:4280–3.

48. Maskens AP. Histogenesis of adenomatous polyps in the human large intestine. Gastroenterology 1979;77:1245–51.

49. Dalerba P, Dylla SJ, Park IK, et al. Phenotypic characterization of human colorectal cancer stem cells. Proc Natl Acad Sci U S A 2007;104:10158–63.

50. Barker N, van Es JH, Kuipers J, et al. Identification of stem cells in small intestine and colon by marker gene Lgr5. Nature 2007;449:1003–7.

How Dysregulated Colonic Crypt Dynamics Cause Stem Cell Overpopulation and Initiate Colon Cancer

Bruce M. Boman, Jeremy Z. Fields, Kenneth L. Cavanaugh, et al.

Cancer Res 2008;68:3304-3313.